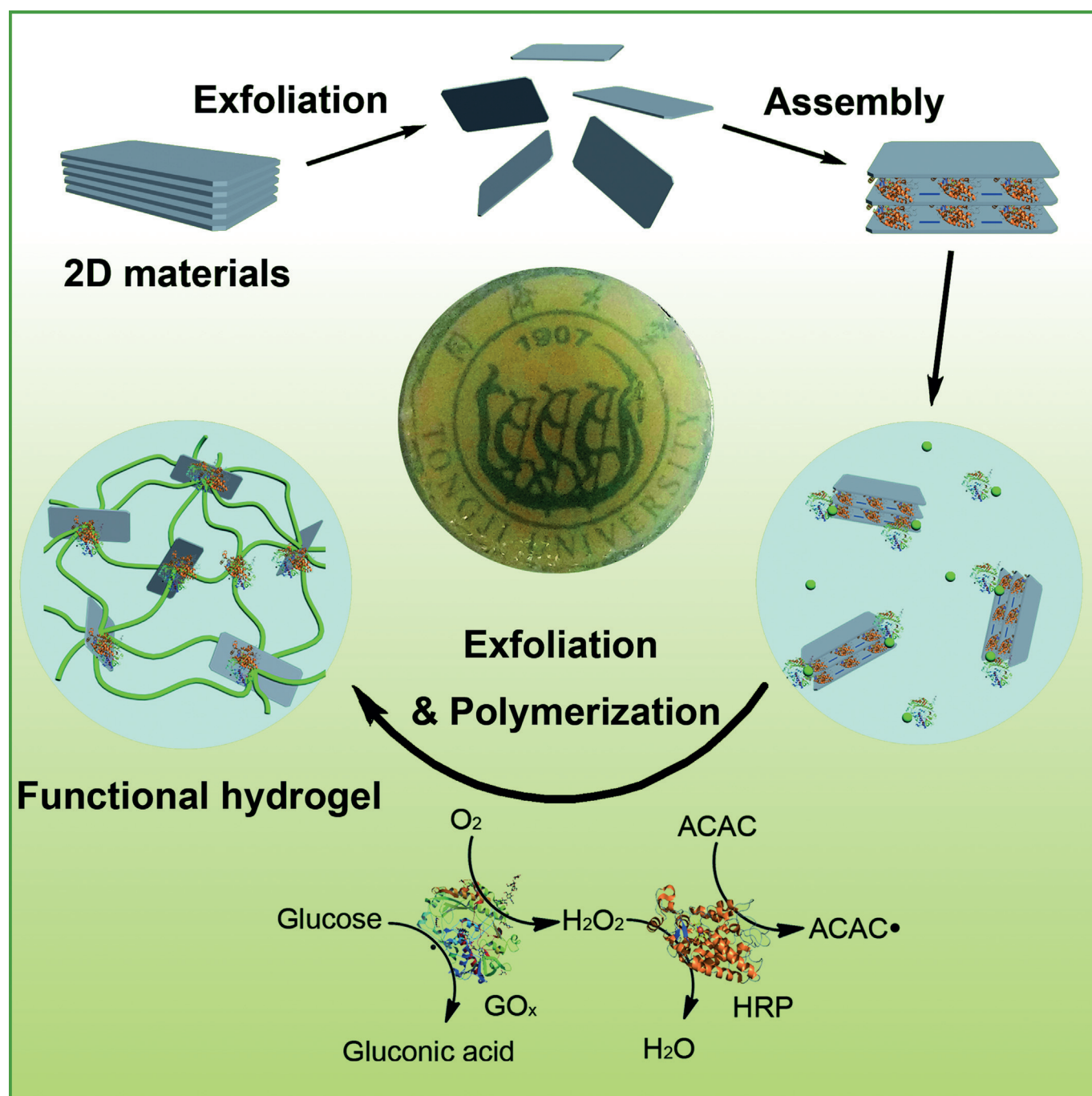


Biocatalysis | *Hot Paper*

Biocatalytic Nanocomposite Hydrogels Formed by HRP-GOx-Cascade-Catalyzed Polymerization and Exfoliation of the Layered Composites**

Chuan-An Liao, Qing Wu, Qing-Cong Wei, and Qi-Gang Wang*[a]



Abstract: The mild preparation of multifunctional nanocomposite hydrogels is of great importance for practical applications. We report that bioinorganic nanocomposite hydrogels, with calcium niobate nanosheets as cross-linkers, can be prepared by dual-enzyme-triggered polymerization and exfoliation of the layered composite. The layered HRP/calcium niobate composites (HRP = horseradish peroxidase) are formed by the assembly of the calcium niobate nanosheets with HRP. The dual-enzyme-triggered polymerization can induce

the subsequent exfoliation of the layered composite and final gelation through the interaction between polymer chains and inorganic nanosheets. The self-immobilized HRP-GOx enzymes (GOx = glucose oxidase) within the nanocomposite hydrogel retain most of enzymatic activity. Evidently, their thermal stability and reusability can be improved. Notably, our strategy could be easily extended to other inorganic layered materials for the fabrication of other functional nanocomposite hydrogels.

Introduction

Hydrogels are a kind of soft material that have been widely applied in industry and biomedical areas due to their porous structure and water-rich microenvironment.^[1] However, traditional hydrogels, either polymers or supramolecular components, always exhibit weak mechanical strength and are limited in real applications.^[2] Haraguchi and co-workers first reported the preparation of tough nanocomposite hydrogels by using clay nanosheets as inorganic cross-linkers.^[3] The ability for these inorganic nanosheets to disperse well in water is necessary to facilitate interactions between the nanosheets and polymer chains.^[4] However, there are few synthetic methods to achieve effective dispersion in nanocomposite systems. One successful method used to prepare tough nylon-clay nanocomposites is the melting-intercalated method.^[5] A similar soft-chemistry exfoliation of an intercalated composite in water should be an effective approach for the in-situ preparation of nanocomposite hydrogels.^[6] With this method, the dispersion difficulties experienced during preparation and purification of the inorganic nanosheets can be avoided. The intercalated composites provide enough inorganic components and have a suitable interlayer space to accommodate monomers for facile exfoliation through polymerization and further gelation by means of three-dimensional crosslinking.^[7] The exploration of a mild polymerization method is another important issue for the in situ preparation of nanocomposite hydrogels. Traditional free-radical polymerizations that occur under thermal conditions, photo or high-energy radiation,^[8] are harmful for the potential biomedical applications, due to the harsh conditions required. This is one reason why enzyme-mediated polymerizations for the preparation of nanocomposite hydrogels have recently become an attractive alternative.^[9] In these studies, horseradish peroxidase (HRP) and hydrogen peroxide form the initiation system that triggers the polymerization of phenol and acrylamide derivatives. Since the excess H₂O₂ may inhibit the biomolecules' functions, H₂O₂ generated in-situ in

the glucose oxidase (GOx)/glucose (Glu) system has been further developed to replace the exogenous H₂O₂.^[10] The gradually generated H₂O₂ can quickly react with HRP, avoiding the detrimental effect of excess H₂O₂.

In this work, a mild method to prepare bioinorganic nanocomposite hydrogels was designed and studied. First, negatively charged calcium niobate (Ca₂Nb₃O₁₀⁻, CNO) nanosheets were generated by exfoliating layered HCa₂Nb₃O₁₀.^[11] The CNO nanosheets were then reassembled with positively charged HRP to form sandwich-structured composites. Upon addition of glucose oxidase, glucose, and acetylacetone (ACAC) to an aqueous solution of these sandwich composites, a HRP-GOx-cascade-catalyzed system is generated and ACAC radicals are produced. These ACAC radicals consequently initiate the polymerization of monomers. The polymerization occurs in the interlayer of the composite and leads to facile exfoliation of layered composite and ultimately to the formation of a nanocomposite hydrogel.

Results and Discussions

A typical nanocomposite hydrogel consists of four components: water, poly (ethylene glycol) methacrylate (PEGMA), CNO nanosheets, and the bio-sourced initiator (Figure 1 a). The prepared CNO nanosheets with an ideal single-layer structure (see Figure S1 in the Supporting Information) were used as cross-linkers. The dual enzymes HRP and GOx were employed to generate ACAC radicals for initiating the polymerization of PEGMA. The detailed preparation of the bioinorganic nanocomposite gel is as follows. First, negatively charged CNO nanosheets self-assembled with positively charged HRP molecules by means of electrostatic interactions form the sandwich-structured HRP-CNO nanocomposite (Figure 1 b). The composite was added to a solution of the PEGMA monomer, GO_x, and ACAC in PBS buffer (20 mM pH 6.0) to form a turbid precursor solution (Figures 1 c and 2 a). Upon vigorous stirring, the monomers diffused into the interlayer of the HRP-CNO nanocomposite. After adding glucose to the buffer, the dual enzymes generated radicals that initiated the polymerization of the monomers. The polymer chains grew from the interlayer of HRP-CNO nanocomposite and gradually exfoliated the structure (Figure 1 d). Lastly, supramolecular interactions between the exfoliated nanosheets and polymer chains lead to the formation of a transparent hydrogel (Figures 1 e and 2 b). The

[a] C.-A. Liao, Q. Wu, Q.-C. Wei, Prof. Dr. Q.-G. Wang
Department of Chemistry, Tongji University
Shanghai 200092 (P. R. China)
E-mail: wangqg66@tongji.edu.cn

[**] HRP = horseradish peroxidase; GOx = glucose oxidase.

Supporting information for this article is available on the WWW under <http://dx.doi.org/10.1002/chem.201501529>.

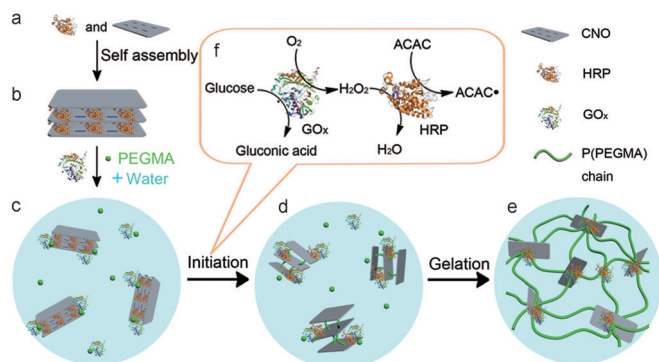


Figure 1. A schematic diagram of the formation of the bio-inorganic nanocomposite hydrogel. a) The starting components used: HRP and CNO nanosheets. b) A sandwich-structured HRP–CNO nanocomposite assembled from electrostatic interaction between HRP and the CNO nanosheets. c) The precursor solution of PEGMA (10 wt%) and HRP–CNO nanocomposite (0.1–1.5 wt %). d) Exfoliation of HRP–CNO nanocomposite during polymerization. e) A 3D network of the final hydrogel. f) A proposed mechanism for the generation of ACAC radicals from the dual-enzyme reaction.

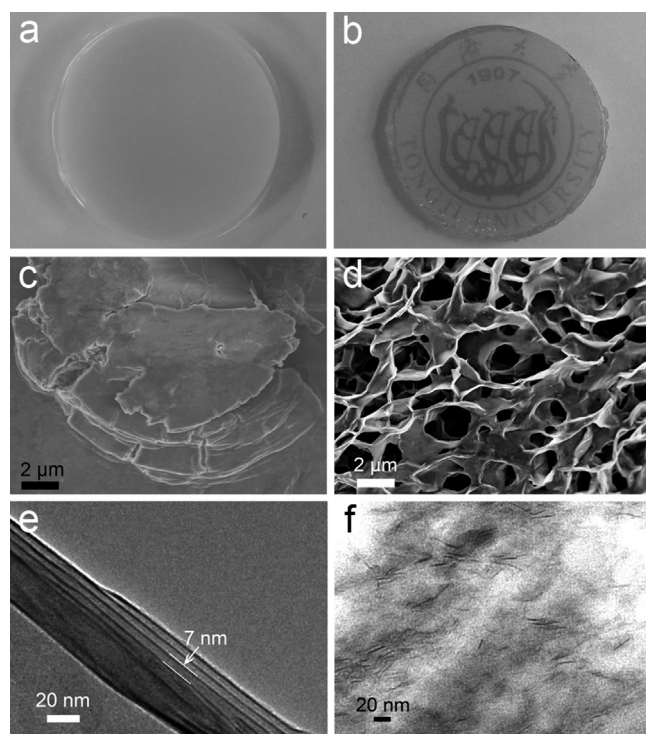


Figure 2. Optical and morphological observations. a) An optical image of the turbid precursor solution. b) An optical image of the final hydrogel. c) An SEM image of the HRP–CNO nanocomposite (HRP/CNO = 2 w/w). d) An SEM image of hydrogel. e) A TEM image of the HRP–CNO nanocomposite (HRP/CNO = 2 (w/w)). f) A TEM image of the hydrogel.

final pH of the hydrogel was about 5.7. The generation of gluconic acid is the main reason for the slightly decreased pH value.

The assembly of the HRP and CNO nanosheets is the key step in our design. From the SEM images (Figure 2c), the HRP–CNO nanocomposite has a slab-like structure with a thickness of tens of micrometers. The assembly of these HRP and CNO

nanosheets is ascribed to the electrostatic attraction of the negatively charged nanosheets and the positively charged HRP. The small-angle X-ray diffraction (SAXD) pattern of the HRP–CNO nanocomposite has a sharp diffraction peak at 1.3° (Figure 3b), which confirms the sandwich structure of nano-

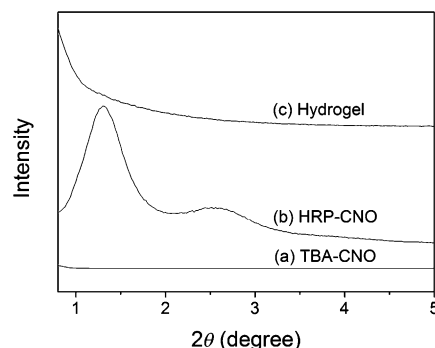


Figure 3. Small-angle X-ray diffraction (SAXD) patterns of a) exfoliated CNO nanosheets, b) HRP–CNO nanocomposite (HRP/CNO = 2 w/w), and c) CNO nanocomposite gel.

composite formed by a layer-by-layer assembly. As a control experiment, the SAXD pattern of exfoliated nanosheets alone has no evident diffraction peak in this region (Figure 3a). From the SAXD results, the interlayer space of the HRP–CNO nanocomposite was calculated to be 6.8 nm by the Bragg equation ($2d\sin\theta = n\lambda$). This value matches the theoretical interlayer space of the HRP–CNO nanocomposite, which was calculated to be between 4.15–7.15 nm, considering a 1.15 nm thick CNO nanosheet^[12] and the dimensions of HRP ($3.0 \times 3.5 \times 6.0$ nm).^[13] The SAXD measured interlayer space indicates that the HRP molecules may arrange within the interlayer at some inclined degree along the long axis dimensions.^[14] The TEM image also shows an intercalated structure for the HRP–CNO nanocomposite with about 1 nm thickness of the inorganic component and about 7 nm space between each layer (Figure 2e). The SAXD and TEM results both confirm a layer-by-layer assembly of HRP molecules and CNO nanosheets. Most importantly, the nanosheets can be enriched more than ten times over the original through this step, so that enough raw materials are available for the following gelation.

The in situ exfoliation and gelation catalyzed by the dual-enzyme-mediated polymerization form the basis of our main proposed mechanism (Figure 1f). First GO_x catalyzes the reaction between the β -D-glucose and oxygen to produce gluconic acid and H_2O_2 (Figure 1f).^[15] The resultant H_2O_2 reacts with the enol form of ACAC to generate carbon-centered radicals during the catalysis of HRP.^[9b,16] As shown in Figure 4, a triplet of doublets in the electron paramagnetic resonance (EPR) spectroscopy confirms the existence of a carbon-centered radical derived from ACAC.^[17] The growth of the polymer chain, which is initiated by ACAC radicals, leads to a gradually exfoliated layered structure of the HRP–CNO nanocomposite. In addition, the SAXD pattern of the gel shows no diffraction peak (Figure 3c), confirming that the layered structure of HRP–CNO

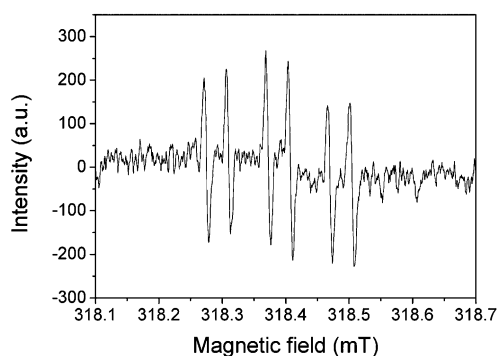


Figure 4. The EPR spectrum of the α -(4-pyridyl-1-oxide)-*N*-tert-butyl nitron (POBN) radical adducts formed in the HRP/GO_x/Glu/ACAC initiation system.

nanocomposite has been exfoliated during the gelation. Finally, the dispersed CNO nanosheets interact with the polymer to form the transparent nanocomposite gel (Figure 2b). The cross-linking in the gel is based on the non-covalent interaction between the exfoliated niobate nanosheets and the polymer chains.^[2b,18] This process is supported by rheological and morphological analysis. The storage modulus (G') is higher than the loss modulus (G'') of the gels, which corroborates the formation of the gel (Figure 5a). As the formation of the physical cross-links is reversible, the gel exhibits a self-recovering property after a large-amplitude oscillatory breakdown (see Figure S2 in the Supporting Information). The SEM image of the gel shows a porous structure with the pore sizes ranging from hundreds of nanometers to several micrometers, indicating the formation of a 3D gel network (Figure 2d). The TEM

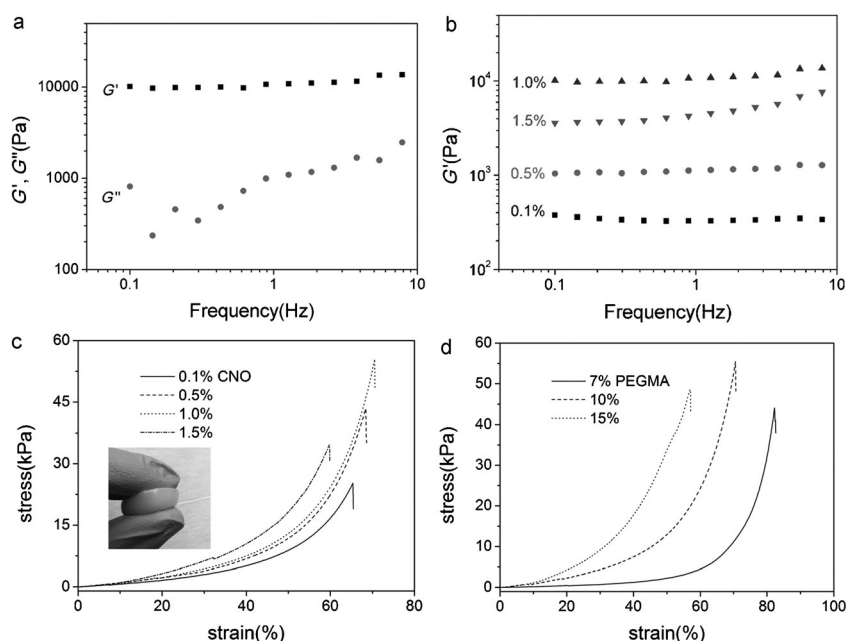


Figure 5. a) Frequency sweep of niobate nanocomposite gel with 1.0% CNO nanosheets and 10% PEGMA. b) The storage modulus (G') values of hydrogels with a CNO nanosheet content varying from 0.1 to 1.5% with a PEGMA content constant (10%). c) Compressive properties the niobate nanocomposite gels with varied concentrations of CNO nanosheets (with constant PEGMA content of 10%, inset: the compressing state of the gel), and d) different PEGMA concentrations (with 1% CNO nanosheets).

images also show the dispersion of the CNO nanosheets within the network of hydrogel (Figure 2f); a mono-dispersed layer of CNO nanosheets in the hydrogel can be seen, indicating that the structure of the HRP-CNO nanocomposite is completely exfoliated due to the dual-enzyme-triggered polymerization.

The bioinorganic nanocomposite gels exhibit excellent mechanical properties. The qualitative analysis results showed that the gel can preserve its integrity under certain compression forces (Figure 5c, inset). The quantitative measurements for mechanical performances of our gel can be described as follows. As shown in Figure 5c and Table S1 (see the Supporting Information), the Young's modulus of gel increased from 0.07 to 0.17 kPa as the amount of CNO nanosheets increased from 0.1 to 1.5%. The broken strain of gel increased from 65 to 71% with an increase of 0.1 to 1.0% of the CNO nanosheets. A further enriched content of CNO nanosheets (1.5%) led to sharply decreased broken strain at 60%. In our system, the nanosheets act as cross-linkers in the bioinorganic nanocomposite gel. The Young's modulus always increased with increasing the density of cross-linking points. However, the excess of inorganic component (above 1.0%) may cause incomplete exfoliation of the HRP-CNO nanocomposite, which would contribute to the ease of breaking after compression. Therefore, the nanosheet content was fixed at 1.0% in the following experiments. The storage modulus changes show the same trends as those of the Young's modulus and compressive strength. As shown in Figure 5b, the storage modulus (G') of the gels has a maximum value of 10.9 kPa with 1.0% CNO. The influence of PEGMA content on the mechanical properties of the gel was further investigated. The Young's modulus was shown to increase from 0.02 to 0.20 kPa as the amount of PEGMA increased from 7 to 15% (Figure 5d). At the same time, the broken strain decreased from 82 to 57% with increasing PEGMA content. It is reasonable that the increased amount of polymer can benefit the compressive modulus. A decreased broken strain along with the increasing polymer content is ascribed to the increased amount of network defects, owing to insufficient interactions between the polymer and the CNO nanosheets. After the comprehensive consideration of the modulus and the broken strain, the amount of PEGMA was fixed at 10%.

The final theme is to study the state of the enzymes after their immobilization within the hydrogel from their mediated

polymerization. The bound enzymes can retain their biocatalytic performance. The oxidation of pyrogallol by H_2O_2 was employed as a model reaction to study the activity of the native and the immobilized enzymes. Both glucose and pyrogallol were used as substrates to carry out a cascade enzymatic reaction. In this reaction, oxygen was converted into H_2O_2 under the GO_x/Glu system, and H_2O_2 further reacted with the pyrogallol to afford purpurogallin under the catalysis of HRP. The activity of the enzymes was measured by monitoring the absorbance at 420 nm by UV/Vis spectroscopy. The average rate in the first minute is defined as initial rate. The HRP and GO_x trapped inside a UV-initiated gel (Gel II) were used as controls for our bi-enzyme-initiated gel (Gel I). As shown in Figure 6a,

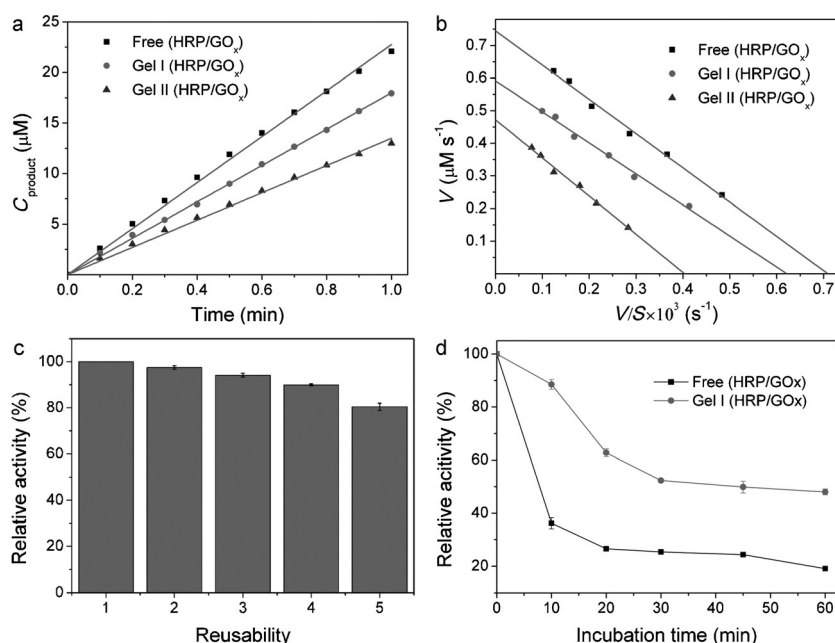


Figure 6. a) The initial reaction curves in the first minute of pyrogallol (10 mM) and glucose (1 mM) catalyzed by various forms of HRP and GO_x in PBS (pH 6.0, 50 mM). b) Eadie-Hofstee plots of the free HRP/ GO_x and immobilized enzymes. c) The relative activities of the immobilized enzyme over the course of five cycles of cascade reactions. d) The retained activities of free and immobilized enzyme after incubation at 60 °C for different times.

the initial rate of the immobilized enzymes in Gel I was about 79% that of the native ones. As a control, the initial rate of the trapped enzymes in Gel II was only 59% that of the native ones.

A kinetic analysis was further used to compare the activities of the enzymes entrapped within the gel and in their native forms. The kinetics of the bi-enzyme catalytic system follows the typical Michaelis–Menten kinetics as for a single enzyme, because the rate-determining step is the catalyzed oxidation of glucose by GO_x . The kinetic constants of the free and immobilized enzymes can be calculated from the Eadie–Hofstee plots between the initial reaction rates at different glucose concentrations (Figure 6b). As shown in Table S2 (see the Supporting Information), the maximum rate (V_{max}) of the self-immobilized enzymes in Gel I ($0.59 \mu\text{M s}^{-1}$) reached 79% that of the native enzymes ($0.75 \mu\text{M s}^{-1}$). The loss of enzyme activity during polymerization is negligible with the rough comparison

of free enzymes after polymerization and free enzymes. Therefore, the loss of the activity can be ascribed to an increased diffusion resistance in the gel network. As a control experiment with a similar gel network, the enzymes in Gel II ($V_{\text{max}} = 0.47 \mu\text{M s}^{-1}$) showed only 63% activity of the native enzymes. Gel II was prepared by a UV-initiated polymerization different to the enzymatic polymerization. The lower activity of the enzymes in Gel II relative to Gel I was ascribed to the possible activity loss of biomolecules under the UV radiation. Therefore, the enzyme-mediated gelation method is more suitable than traditional UV-initiated gelation method.

In general, enzymes are effective catalysts with high efficiencies and excellent selectivity. The immobilized carriers are important for potential industrial applications of enzymes due to the facile reusability, high stability and retained catalytic efficiency.^[19] One advantage of our hydrogel-immobilized enzymes is their reusability. In order to reuse the immobilized enzymes, the gel was washed three times after the oxidation of pyrogallol in each run. As seen in Figure 6c, the enzymes in the gel retained 80% activity after five cycles. Another advantage of the bioinorganic hydrogel-bound enzymes is their thermal stability imparted by the protective inorganic component. The free and immobilized enzymes were incubated at 60 °C in PBS (pH 6.0, 50 mM) for different times before testing their activity. The enzymes in the gel maintained 48% of their initial activity after incubation at 60 °C for 60 min, while the free enzymes retained only 19% under the same conditions (Figure 6d). The inorganic component in the hydrogel can hinder the destruction of the proteins and therefore reduce the denaturalization of the enzymes.

Conclusion

In summary, we have prepared niobate nanocomposite hydrogels through dual-enzyme-triggered polymerization and exfoliation of the layered niobate composite. During polymerization, the growth of the polymer chain gradually destroyed the layered structure of HRP–CNO nanocomposite. The homogeneously dispersed inorganic nanosheets within the nanocomposite gel provide desirable mechanical properties. The self-immobilized HRP– GO_x enzymes within the nanocomposite hydrogel retained most of their enzymatic activity even several cycles of use. The protection of the niobate nanosheets can enhance the thermal stability of the enzymes. Notably, our

strategy could be easily extended to other kind of nanosheets for multi-functional nanocomposite hydrogels.

Experimental Section

Materials

Horseradish peroxidase (HRP, EC 1.11.1.7, MW = 40 kDa, 300 U mg⁻¹) was purchased from Shanghai Baoman Biotechnology Co., Ltd. Glucose oxidase from *Aspergillus niger* (MW = 160 kDa, EC 1.1.3.4, lyophilized powder), PEGMA (average Mn 360) were obtained from Sigma-Aldrich. K₂CO₃, CaCO₃, Nb₂O₅, acetic acid (HAc), and glucose were obtained from Sinopharm Chemical Reagent Co., Ltd. All materials and reagents were analytical grade and used as received.

Preparation of the CNO nanosheets

A colloidal suspension of CNO nanosheets was prepared according to previous reports with minor modifications.^[11] Firstly, K₂CO₃, CaCO₃ and Nb₂O₅ (stoichiometric ratio K/Ca/Nb = 1.2:2:3) were combined and heated at 1473 K for 12 h in air to obtain the layered calcium niobate KCa₂Nb₃O₁₀. Then the KCa₂Nb₃O₁₀ powder was incubated in 5.0 M HNO₃ (1 g per 100 mL) for 72 h with stirring and filtered. By repeating the above acidification twice, the proton derivative HCa₂Nb₃O₁₀ was obtained. The HCa₂Nb₃O₁₀ (0.6 g) was dispersed in 150 mL of tetrabutylammonium hydroxide (TBAOH) solution (with 1:1 molar ratio of TBA⁺/H⁺). After stirring for 7 days, the colloidal suspension of CNO nanosheets (2 mg mL⁻¹) was obtained by centrifuging at 8000 rpm and removing the sediment.

Preparation of nanocomposite hydrogels

In a typical gelation, the HRP solution (0.5 mL, 10 mg mL⁻¹) was mixed with the previous colloidal suspension of CNO nanosheets (1 mL). Reddish HRP-CNO nanocomposites precipitated quickly upon addition of the dilute acetic acid to pH 5.0. The composite was washed with distilled water three times to remove non-immobilized HRP. The composite (5.6 mg) was mixed with a 20 mM pH 6.0 PBS buffer solution of PEGMA monomer (0.14–0.30 g), GOx (10 mg mL⁻¹, 0.1 mL), and ACAC (20 μL) to form translucent precursors (2.0 g). After the addition of glucose (2.5 mM), the precursor solution gradually formed a transparent nanocomposite hydrogel during 2 h enzymatic reaction at 30 °C. The control gel with the same components and enzymes was formed by the CNO-initiated polymerization under 1 h UV irradiation (average intensity of 2.0 mW cm⁻² at 365 nm).

Characterization

XRD patterns were obtained on a Bruker Focus D8 diffractometer with Cu_{Kα} radiation (α = 1.5408). The wide X-ray powder diffraction was measured from 10 to 70° with the scanning rate of 0.1 s step⁻¹ with an increment of 0.02. Small-angle X-ray diffraction was performed from 0.8 to 5° with the scanning rate of 0.5° min⁻¹. Compressive tests on gels were performed with a FR-108B tensile-compressive tester (Farui Co.). Cylindrical gel samples of 16 mm in diameter and about 6 mm in thickness were compressed at a constant cross-head speed of 1 mm min⁻¹. The SEM samples were pre-treated by freeze drying and gold sputtering, and then observed by a scanning electron microscope (Hitachi S-4800) at a voltage of 1 kV. The TEM graphics of the inorganic species were obtained by transmission electron microscopy (JEM-2100) at a 200 kV accelerating voltage. The TEM images of the bio-cut hydrogels were ac-

quired by JEM-2010 transmission electron microscopy (TEM) at an accelerating voltage of 80 kV. Rheological measurements of the hydrogels were performed with a RS6000 rheometer (Haake Instruments) with a parallel plate (20 mm diameter, 0.40 mm gap) at 25 °C. Frequency sweeps were carried out to measure the storage modulus (*G'*) and loss modulus (*G''*) at a constant strain of 1.0 Pa.

Test of catalytic activity

The oxidation of pyrogallol by H₂O₂ was used as a model reaction to assess the catalytic activity of the immobilized and free HRP/GOx. In a typical experiment, buffer solution (2 mL, 50 mM, pH 7.0) containing pyrogallol (10 mM) and glucose (0.5–5 mM) was mixed with HRP (9 μg mL⁻¹) and GOx (2.5 μg mL⁻¹), or a piece of hydrogel containing the same amount of enzymes. The change of absorbance at 420 nm, the absorption peak of the oxidation product purpurogallin, was measured by using the dynamic mode of a UV/Vis spectrometer (UV-2700, Shimadzu) with 6 s intervals. The slope in the first minute was used to calculate the initial reaction rate. Kinetic constants were determined from the corresponding Eadie-Hofstee plots.

Acknowledgements

We thank the support of the National Natural Science Foundation of China (21274111, 51473123, 51402215), the Program for New Century Excellent Talents in University of Ministry of Education of China (NECT-11-0386), the China Postdoctoral Science Foundation (2014M550245), the Shanghai Postdoctoral Science Foundation (14R21411200), and the Recruitment Program of Global Experts.

Keywords: biocatalysis · calcium niobate · domino reactions · nanocomposite hydrogel · radical polymerization

- [1] a) Y. Liu, T. Wang, M. Liu, *Chem. Eur. J.* **2012**, *18*, 14650–14659; b) L. Cao, B. Cao, C. Lu, G. Wang, L. Yu, J. Ding, *J. Mater. Chem. B* **2015**, *3*, 1268–1280; c) J. R. McKee, E. A. Appel, J. Seitsonen, E. Kontturi, O. A. Scherman, O. Ikkala, *Adv. Funct. Mater.* **2014**, *24*, 2706–2713; d) K. L. Morris, L. Chen, J. Raeburn, O. R. Sellick, P. Cotanda, A. Paul, P. C. Griffiths, S. M. King, R. K. O'Reilly, L. C. Serpell, D. J. Adams, *Nat. Commun.* **2013**, *4*, 1480; e) S. Van Vlierberghe, P. Dubruel, E. Schacht, *Biomacromolecules* **2011**, *12*, 1387–1408; f) X. Ji, S. Dong, P. Wei, D. Xia, F. Huang, *Adv. Mater.* **2013**, *25*, 5725–5729; g) L. Qin, F. Xie, P. Duan, M. Liu, *Chem. Eur. J.* **2014**, *20*, 15419–15425; h) Z. Xue, S. Wang, L. Lin, L. Chen, M. Liu, L. Feng, L. Jiang, *Adv. Mater.* **2011**, *23*, 4270–4273.
- [2] a) L. A. Estroff, A. D. Hamilton, *Chem. Rev.* **2004**, *104*, 1201–1218; b) K. Haraguchi, *Polym. J.* **2011**, *43*, 223–241; c) C.-J. Wu, A. K. Gaharwar, B. K. Chan, G. Schmidt, *Macromolecules* **2011**, *44*, 8215–8224; d) Z. Yang, G. Liang, B. Xu, *Acc. Chem. Res.* **2008**, *41*, 315–326.
- [3] K. Haraguchi, T. Takehisa, *Adv. Mater.* **2002**, *14*, 1120–1124.
- [4] a) J. Liang, Y. Huang, L. Zhang, Y. Wang, Y. Ma, T. Guo, Y. Chen, *Adv. Funct. Mater.* **2009**, *19*, 2297–2302; b) D. Paul, L. Robeson, *Polymer* **2008**, *49*, 3187–3204; c) J. R. Potts, D. R. Dreyer, C. W. Bielawski, R. S. Ruoff, *Polymer* **2011**, *52*, 5–25.
- [5] a) J. Cho, D. Paul, *Polymer* **2001**, *42*, 1083–1094; b) Y. Kojima, A. Usuki, M. Kawasumi, A. Okada, Y. Fukushima, T. Kurauchi, O. Kamigaito, *J. Mater. Res.* **1993**, *8*, 1185–1189; c) A. Usuki, Y. Kojima, M. Kawasumi, A. Okada, Y. Fukushima, T. Kurauchi, O. Kamigaito, *J. Mater. Res.* **1993**, *8*, 1179–1184.
- [6] C. Liao, Q. Wu, T. Su, D. Zhang, Q. Wu, Q. Wang, *ACS Appl. Mater. Interfaces* **2014**, *6*, 1356–1360.

- [7] a) A. V. Powell, L. Kosidowski, A. McDowall, *J. Mater. Chem.* **2001**, *11*, 1086–1091; b) R. Ma, X. Liu, J. Liang, Y. Bando, T. Sasaki, *Adv. Mater.* **2014**, *26*, 4173–4178.
- [8] a) A. M. Jonker, D. W. Löwik, J. C. van Hest, *Chem. Mater.* **2012**, *24*, 759–773; b) P. Shestakova, R. Willem, E. Vassileva, *Chem. Eur. J.* **2011**, *17*, 14867–14877; c) Y.-J. Lin, G.-H. Lee, C.-W. Chou, Y.-P. Chen, T.-H. Wu, H.-R. Lin, *J. Mater. Chem. B* **2015**, *3*, 1931–1941; d) M. Liu, Y. Ishida, Y. Ebina, T. Sasaki, T. Aida, *Nat. Commun.* **2013**, *4*, 2029; e) Q. Wu, T. Su, Y. Mao, Q. Wang, *Chem. Commun.* **2013**, *49*, 11299–11301; f) D. Zhang, J. Yang, S. Bao, Q. Wu, Q. Wang, *Sci. Rep.* **2013**, *50*, 1399; g) J. Zhao, X. Zhao, B. Guo, P. X. Ma, *Biomacromolecules* **2014**, *15*, 3246–3252.
- [9] a) T. Su, Z. Tang, H. He, W. Li, X. Wang, C. Liao, Y. Sun, Q. Wang, *Chem. Sci.* **2014**, *5*, 4204–4209; b) T. Su, D. Zhang, Z. Tang, Q. Wu, Q. Wang, *Chem. Commun.* **2013**, *49*, 8033–8035; c) M. Kurisawa, J. E. Chung, Y. Y. Yang, S. J. Gao, H. Uyama, *Chem. Commun.* **2005**, 4312–4314; d) N. Q. Tran, Y. K. Joung, E. Lih, K. D. Park, *Biomacromolecules* **2011**, *12*, 2872–2880; e) K. Moriyama, K. Minamihata, R. Wakabayashi, M. Goto, N. Kamiya, *Chem. Commun.* **2014**, *50*, 5895–5898; f) B. P. Partlow, C. W. Hanna, J. Rnjak-Kovacina, J. E. Moreau, M. B. Applegate, K. A. Burke, B. Marelli, A. N. Mitropoulos, F. G. Omenetto, D. L. Kaplan, *Adv. Funct. Mater.* **2014**, *24*, 4615–4624.
- [10] a) S. Sakai, K. Komatani, M. Taya, *RSC Advances* **2012**, *2*, 1502–1507; b) S. Sakai, M. Tsumura, M. Inoue, Y. Koga, K. Fukano, M. Taya, *J. Mater. Chem. B* **2013**, *1*, 5067–5075.
- [11] a) L. Gao, Q. Gao, Q. Wang, S. Peng, J. Shi, *Biomaterials* **2005**, *26*, 5267–5275; b) A. Jacobson, J. W. Johnson, J. Lewandowski, *Inorg. Chem.* **1985**, *24*, 3727–3729.
- [12] a) L. Chang, M. A. Holmes, M. Waller, F. E. Osterloh, A. J. Moulé, *J. Mater. Chem.* **2012**, *22*, 20443–20450; b) A. Jacobson, J. Lewandowski, J. W. Johnson, *J. Less-Common Met.* **1986**, *116*, 137–146; c) C. Sun, P. Peng, L. Zhu, W. Zheng, Y. Zhao, *Eur. J. Inorg. Chem.* **2008**, 3864–3870.
- [13] a) W.-Y. Cai, Q. Xu, X.-N. Zhao, J.-J. Zhu, H.-Y. Chen, *Chem. Mater.* **2006**, *18*, 279–284; b) K. Kamada, S. Tsukahara, N. Soh, *J. Phys. Chem. C* **2011**, *115*, 13232–13235; c) L. Zhang, Q. Zhang, X. Lu, J. Li, *Biosens. Bioelectron.* **2007**, *23*, 102–106.
- [14] a) C. Kumar, A. Chaudhari, *Chem. Mater.* **2001**, *13*, 238–240; b) S. Peng, Q. Gao, Q. Wang, J. Shi, *Chem. Mater.* **2004**, *16*, 2675–2684.
- [15] a) S. Kobayashi, H. Uyama, S. Kimura, *Chem. Rev.* **2001**, *101*, 3793–3818; b) H. Uyama, H. Kurioka, S. Kobayashi, *Polym. J.* **1997**, *29*, 190–192.
- [16] a) M. Kohri, A. Kobayashi, H. Fukushima, T. Kojima, T. Taniguchi, K. Saito, T. Nakahira, *Polym. Chem.* **2012**, *3*, 900–906; b) A. Singh, D. Ma, D. L. Kaplan, *Biomacromolecules* **2000**, *1*, 592–596; c) A. Durand, T. Lalot, M. Brigodiot, E. Maréchal, *Polymer* **2000**, *41*, 8183–8192; d) T. Lalot, M. Brigodiot, E. Maréchal, *Polym. Int.* **1999**, *48*, 288–292.
- [17] K. Iwahara, M. Hirata, Y. Honda, T. Watanabe, M. Kuwahara, *Biotechnol. Lett.* **2000**, *22*, 1355–1361.
- [18] Y.-S. Han, J.-H. Choy, *J. Mater. Chem.* **2001**, *11*, 1277–1282.
- [19] a) O. Barbosa, R. Torres, C. Ortiz, A. N. Berenguer-Murcia, R. C. Rodrigues, R. Fernandez-Lafuente, *Biomacromolecules* **2013**, *14*, 2433–2462; b) A. Liese, L. Hilterhaus, *Chem. Soc. Rev.* **2013**, *42*, 6236–6249.

Received: April 20, 2015
Published online on July 31, 2015